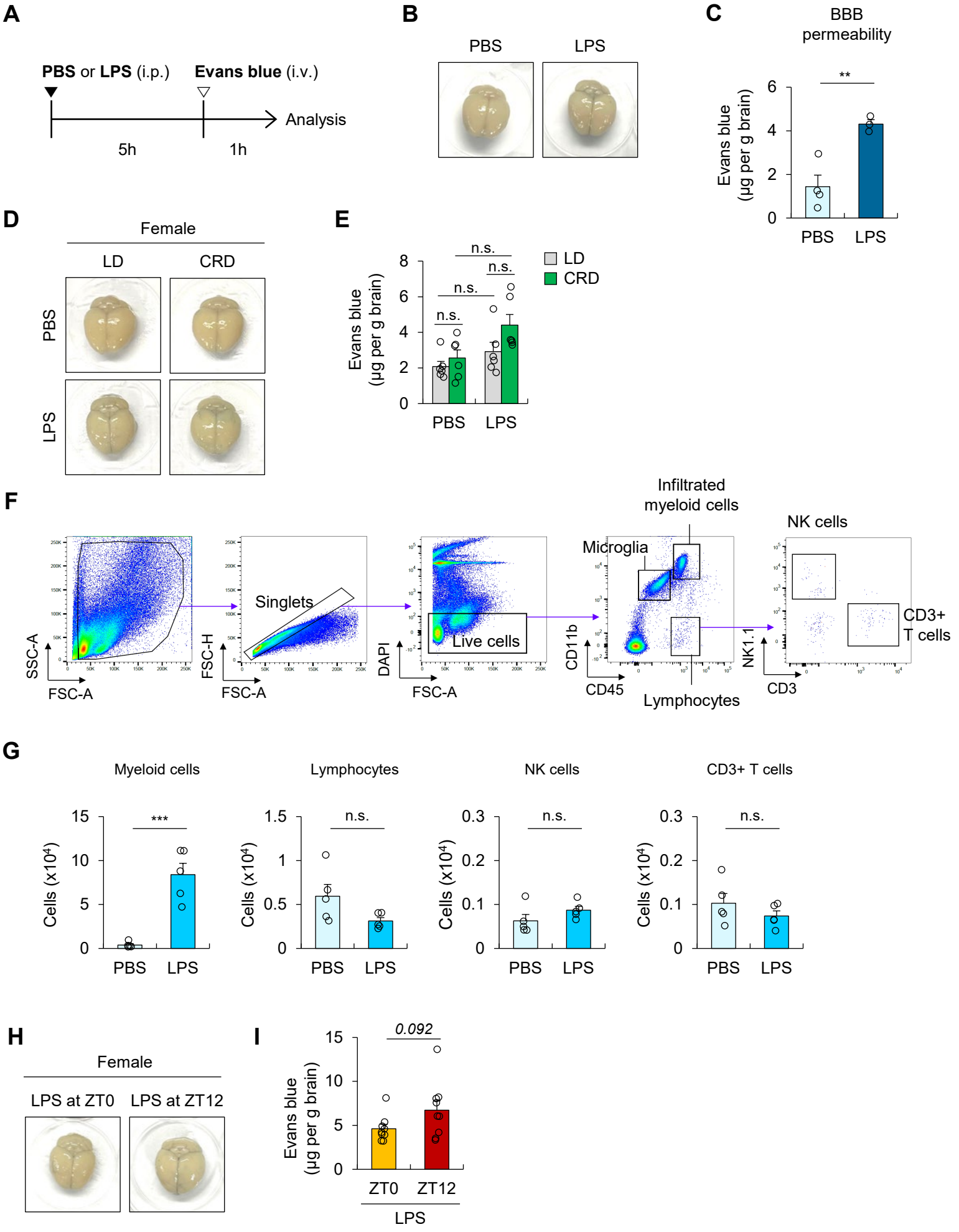

Supplementary Figure S1. Circadian rhythm-dependent modulation of BBB permeability during systemic inflammation.

(A) Experimental scheme of BBB permeability assay. PBS or LPS (4 mg/kg) was administrated to male mice, and Evans blue was injected intravenously 1 h before brain tissue collection. (n = 4 per group) (B, C) Representative brain images (B) and quantification (C) of Evans blue dye in brain tissues. (n = 4, PBS group; n = 3, LPS group) (D, E) Representative brain images (D) and quantification (E) of Evans blue extravasation in female mice treated with PBS or LPS (4 mg/kg) under LD or CRD conditions as shown in Fig. 1A. (n = 6 per group) (F, G) Gating strategy (F) and quantification of immune cells (G) in the brain tissues of LPS-treated mice by flow cytometry. (n = 5, PBS; n = 5, LPS) (H, I) Representative brain images (H) and quantification (I) of Evans blue leakage in female mice after LPS (2.5 mg/kg) injection at ZT0 or ZT12 (n = 9 per group). $^{**}P < 0.01$, $^{***}P < 0.001$, n.s. not significant.

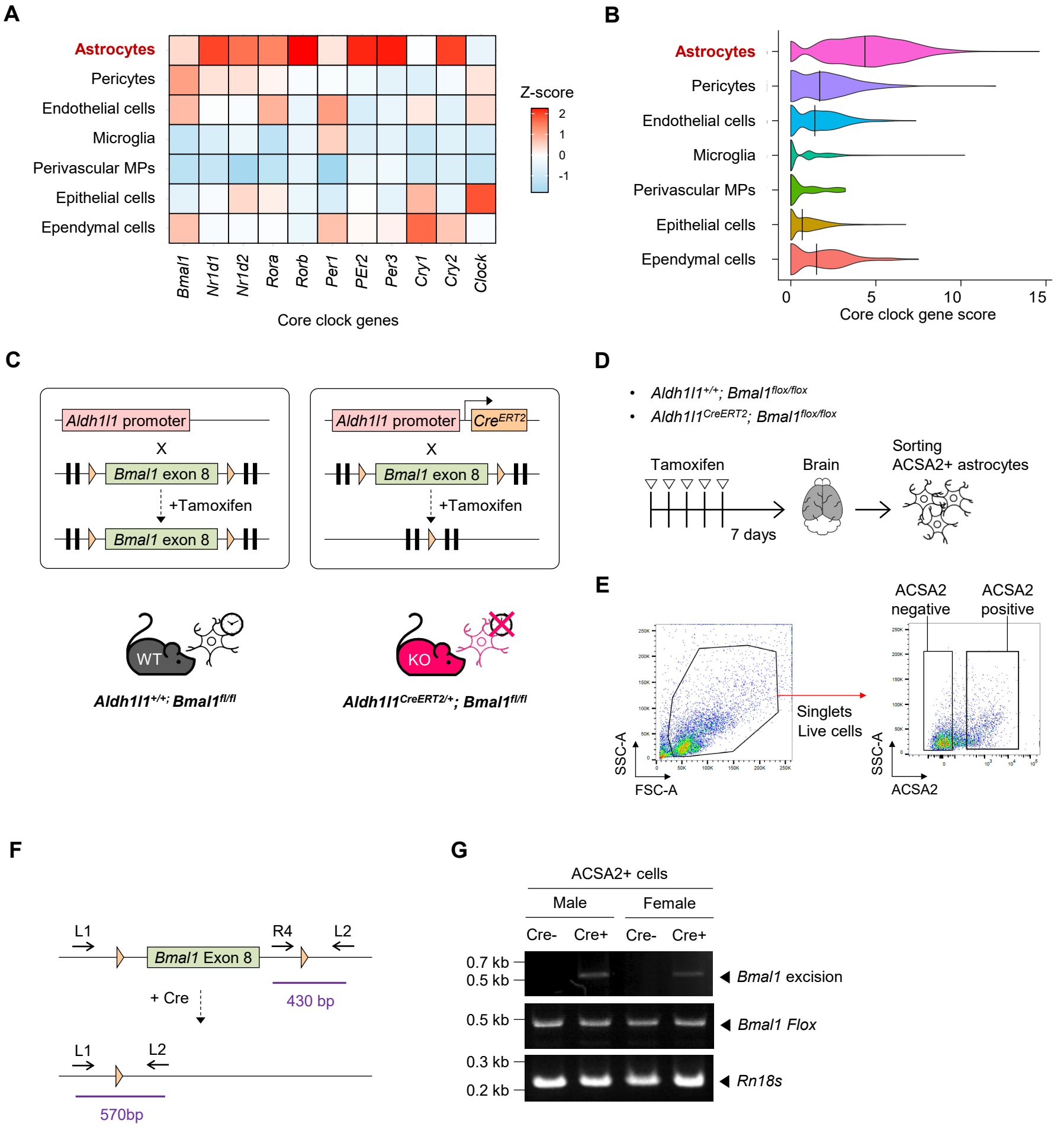

Supplementary Figure S2. Single cell RNA-seq analysis on the core clock gene expression and validation of astrocyte-specific *Bmal1* ablation in mice.

(A, B) Reanalysis of expression pattern of core clock genes in the brain cell-types using mouse brain single-cell RNA sequencing dataset (GSE263094). (A) A heatmap shows the proportion of brain cell populations expressing core clock genes. (B) A violin plot presents the CCG score calculated from the total normalized expression of core clock genes. (C) Schematic illustration of astrocyte-specific *Bmal1*–deficient mice generation. (D) Experimental scheme of mouse brain and ACSA2+ astrocytes isolation. (E) FACS gating strategy for ACSA2+ astrocytes sorting. (F) Schematic illustration of genotyping strategy showing primer binding sites and expected product sizes. (G) PCR products from sorted ACSA2+ astrocytes confirm the conditional knockout in AS-B1KO compared with CTRL.

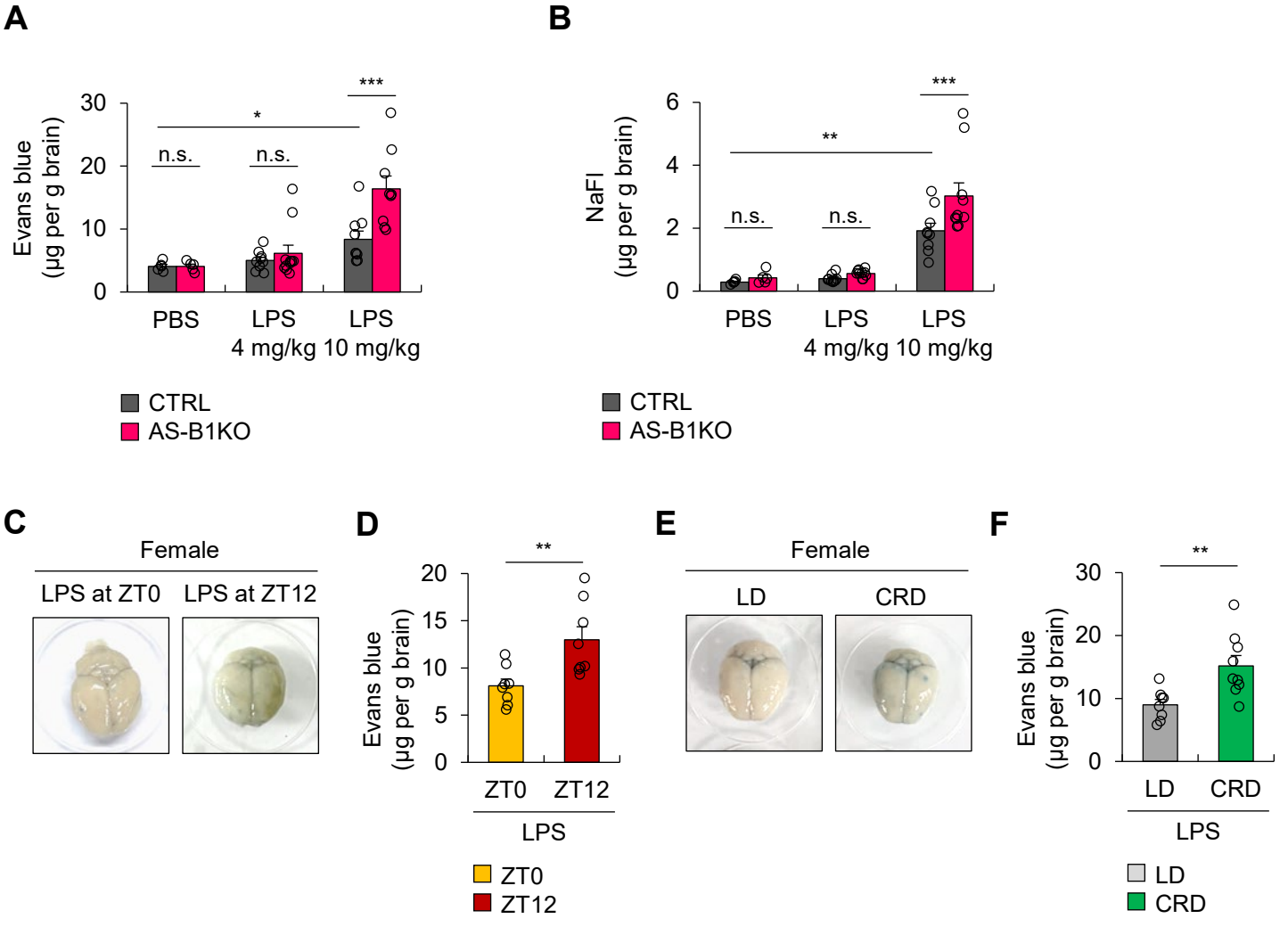

Supplementary Figure S3. Astrocytic *Bmal1* deficiency or circadian rhythm influences BBB integrity of female mice in response to higher LPS administration.

(A, B) Quantification of Evans blue (A) and NaFl (B) in female control and astrocytic *Bmal1*-kncokout mice treated with PBS or LPS (4, or 10 mg/kg). (A) Evans blue, n = 5, PBS group; n = 9, CTRL-LPS 4mg/kg; n = 9, CTRL-LPS 10 mg/kg; n = 11, AS-B1KO-LPS 4 mg/kg; n = 9, AS-B1KO-LPS 10 mg/kg. (B) NaFl, n = 5, PBS group; n = 9, CTRL-LPS group; n = 10, AS-B1KO-LPS group. (C, D) Representative brain images (C) and quantification (D) of Evans blue extravasation in female mice treated with LPS (10 mg/kg) at ZT0 or ZT 12 (n = 8 per group). (E, F) Representative brain images (E) and quantification (F) of Evans blue leakage in female mice after LPS (10 mg/kg) injection under LD or CRD conditions as shown in Fig. 1A. (n = 8, LD-LPS; n = 9, CRD-LPS). Asterisks indicate significant differences. *P < 0.05, **P < 0.01, ***P < 0.001, n.s. not significant.

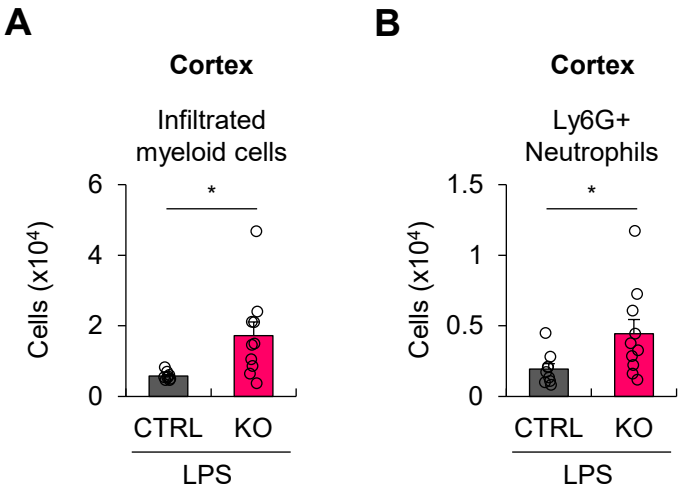

Supplementary Figure S4. Astrocyte *Bmal1* deficiency increases neutrophil infiltration into cortex following LPS challenge.

(A-B) Quantification of brain-infiltrating myeloid cells (A) and Ly6G+ neutrophils (B) in the cortex of control and astrocytic Bmal1 knockout mice after 24 h LPS injection. (n = 9, CTRL-LPS; n = 10, KO-LPS). Asterisks indicate significant differences. *$P < 0.05$.

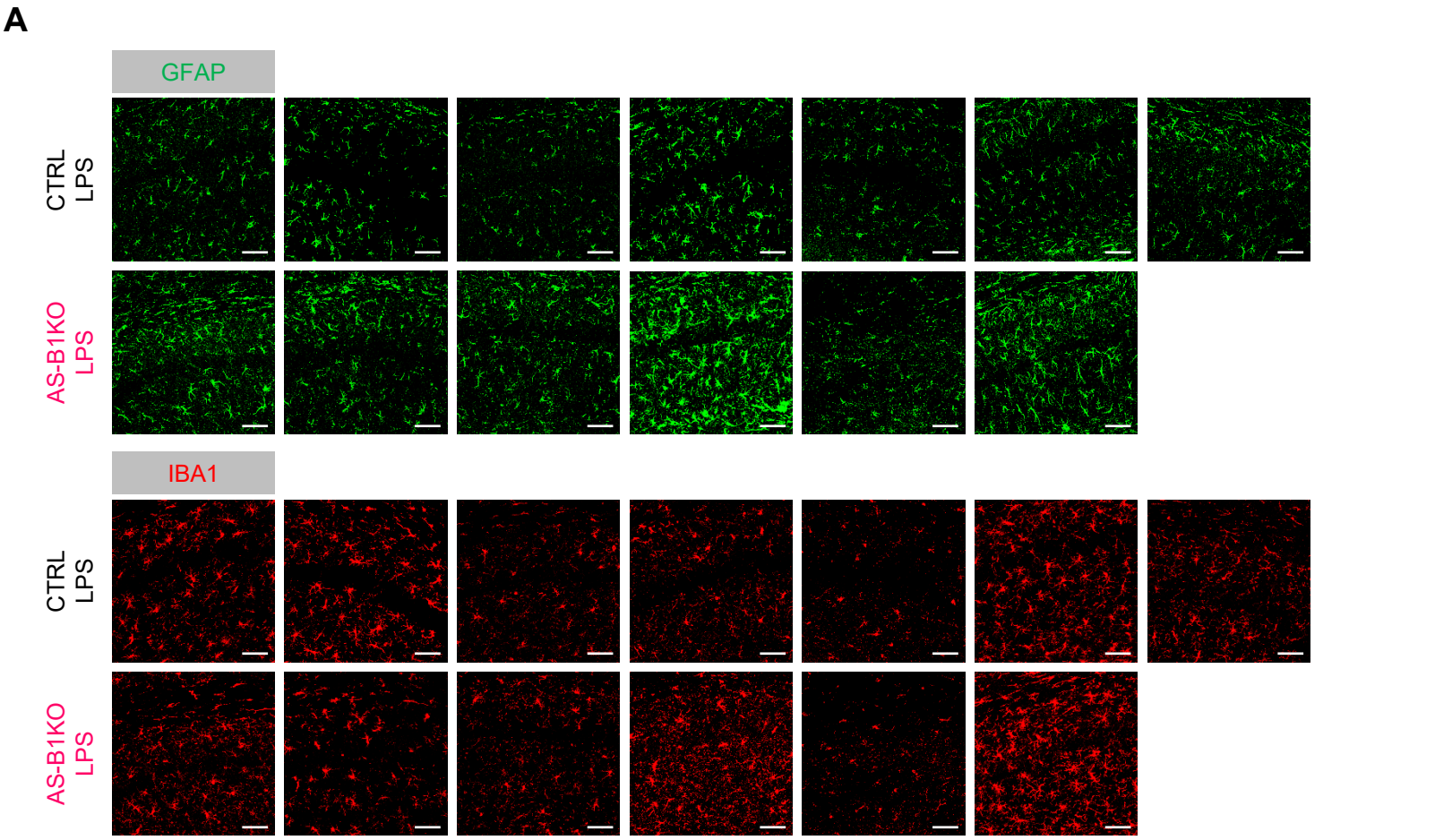

Supplementary Figure S5. Analysis of astrocyte alterations in astrocytic *Bmal1*-deficient mice following LPS challenge.

(A) Confocal immunofluorescence images showing GFAP+ astrocytes (green) and IBA1+ microglia (red) in hippocampal sections of control and astrocytic *Bmal1* KO mice at 24 h post-LPS (n = 7, CTRL-LPS; n = 6, AS-B1KO-LPS). Scale bar, 50 μm. (B) Representative high-magnification image of hippocampal astrocyte (upper panel) and its skeletonized morphology (lower panel) of control and astrocytic *Bmal1* KO mice 24 h after LPS injection. Scale bar, 10 μm. (C, D) Quantification of maximum branch length (C) and number of branches (D) derived from skeletonized astrocytes as in (B). Each data point represents the mean of 10 cells per mouse. (n = 7, CTRL-LPS; n = 6, AS-B1KO-LPS) (E) Quantification of *Gfap* mRNA assessed by qPCR in brain homogenates from CTRL and AS-B1KO mice 24 h post-LPS challenge. (n = 6) Asterisks indicate significant differences. *P < 0.05, **P < 0.01, n.s. not significant.

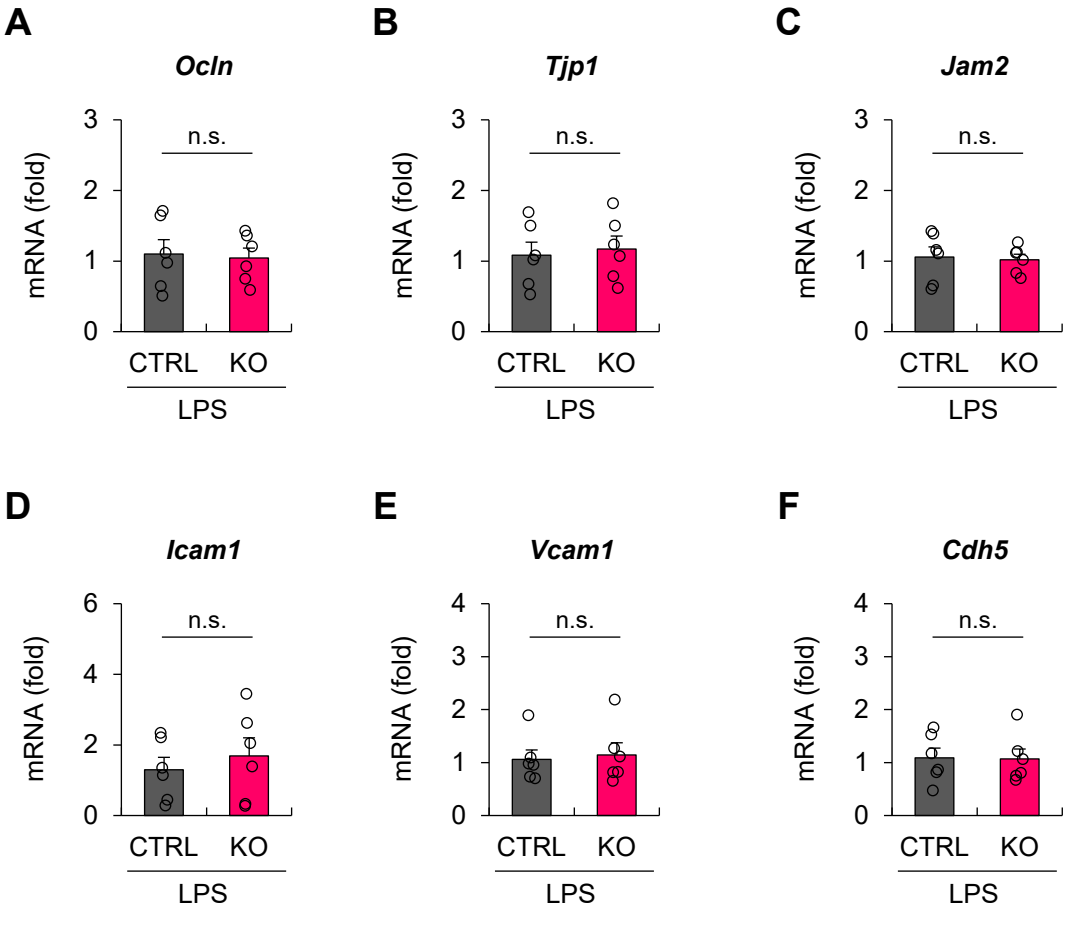

Supplementary Figure S6. Tight junction gene and adhesion molecule expression is not altered in brain tissue of astrocytic *Bmal1*-deficient mice.

(A-C) Expression levels of tight junctions (*Ocln*, *Tjp1*, *Jam2*) and (D-F) adhesion molecules (*Icam1*, *Vcam1*, *Cdh5*) in brain tissue from CTRL and AS-B1KO mice 24 h after LPS injection (n = 6 per group). n.s. not significant.

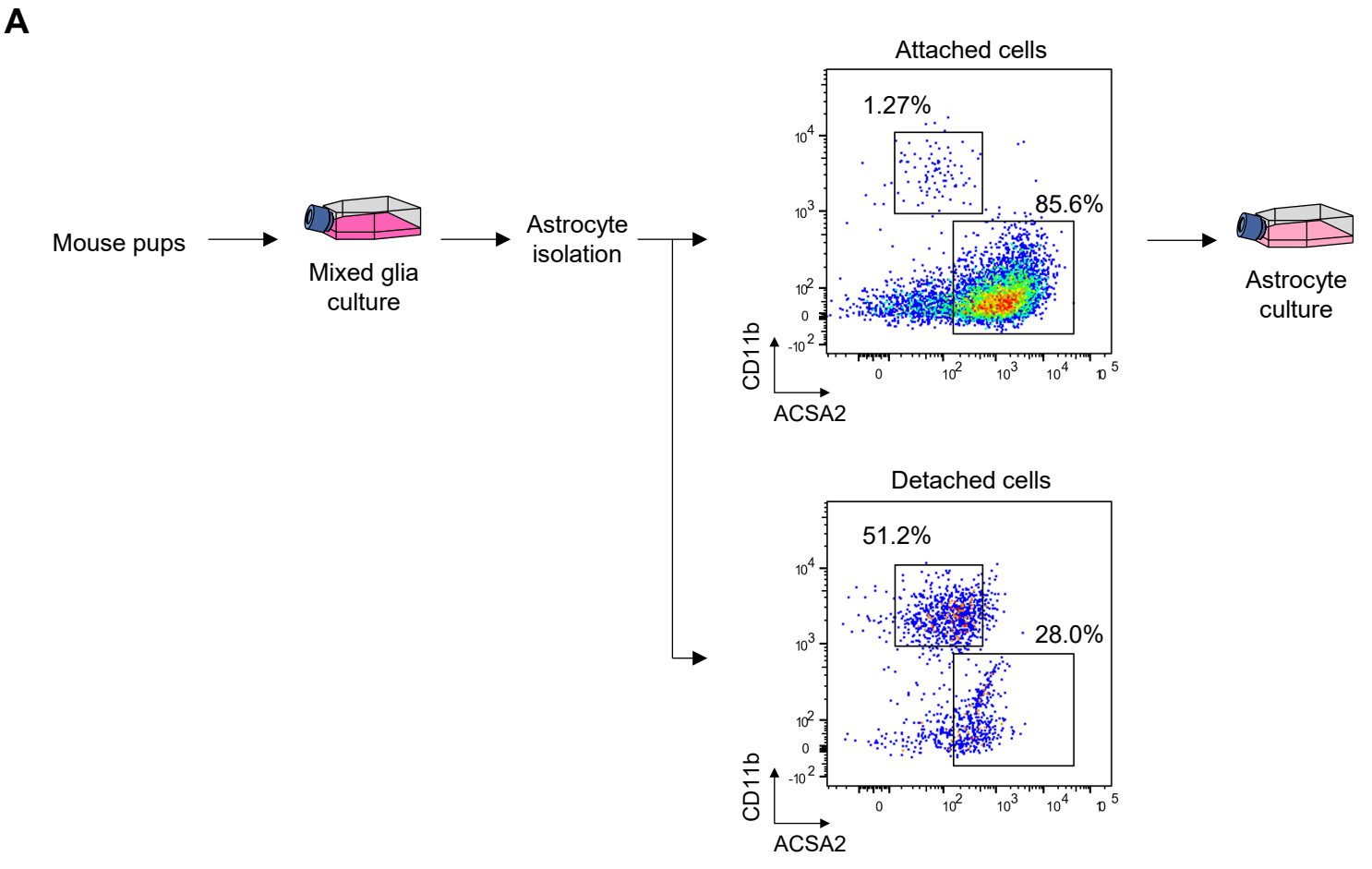

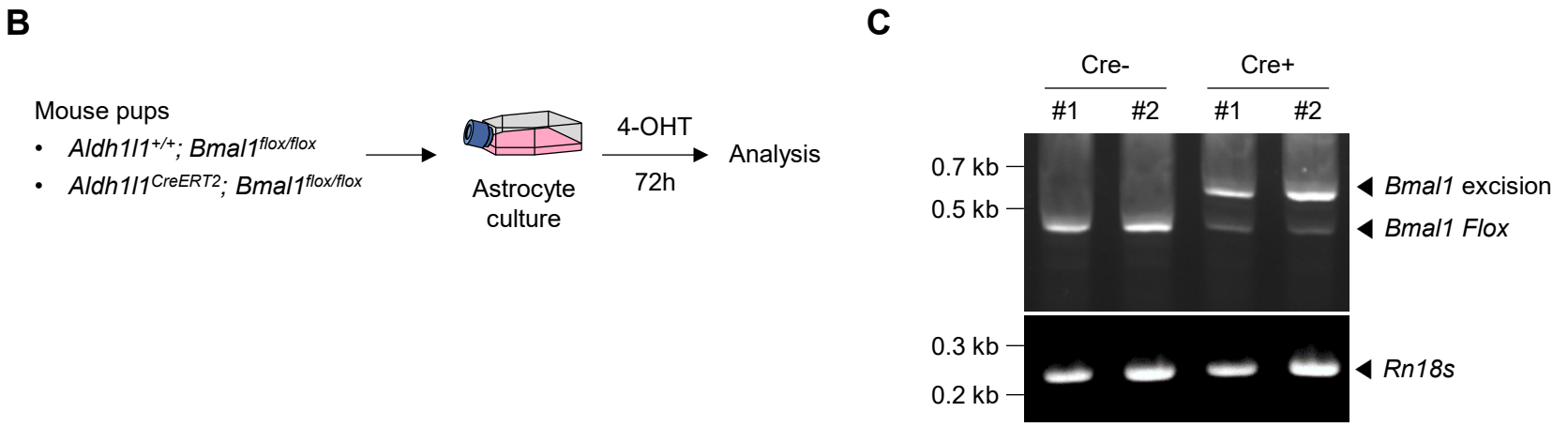

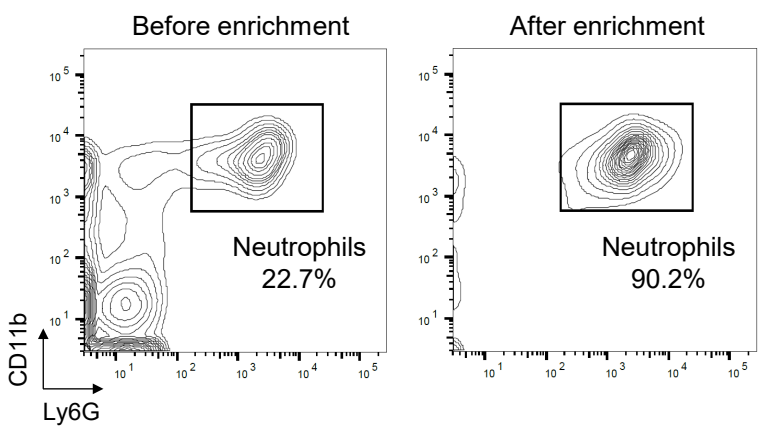

Supplementary Figure S7. Establishment of *Bmal1*-deficient astrocyte culture and validation of neutrophil enrichment.

(A) Schematic illustration for primary astrocyte culture from mouse pups. (B) Primary astrocyte cultures from Bmal1$^{flox/flox}$ or Aldh1l1^{CreERT2};Bmal1$^{flox/flox}$ mice were treated with 4-OHT to induce Cre-mediated excision of *Bmal1* exon. (C) Bmal1 knockout was verified by genotyping. (D) Representative flow cytometric dot plots identifying neutrophil population before and after enrichment.

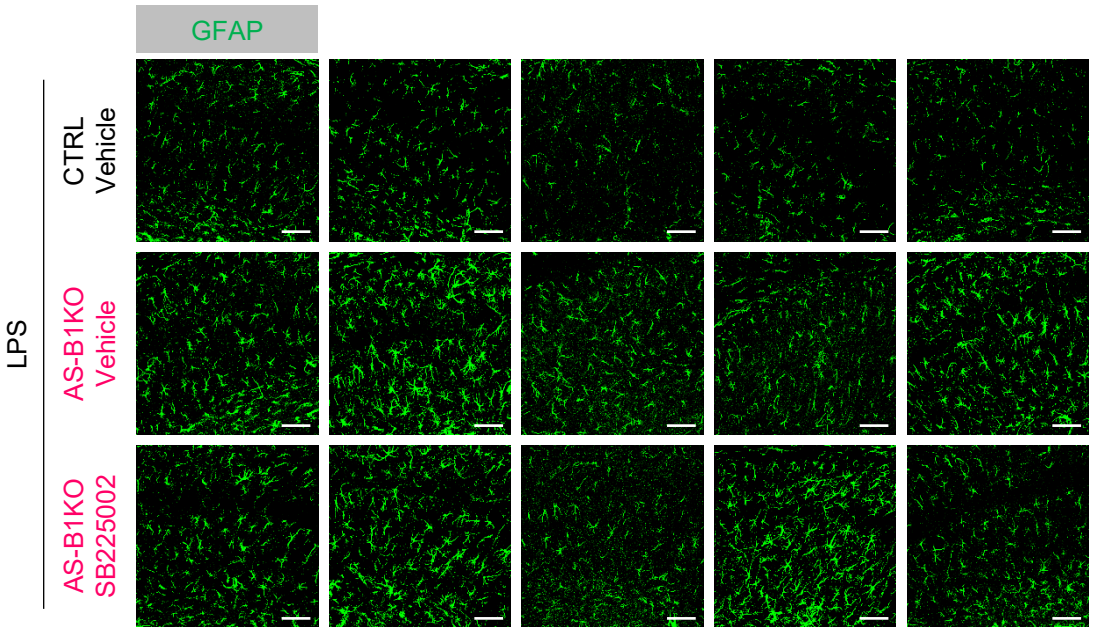

Supplementary Figure S8. CXCR2 blockade does not alter hippocampal astrogliosis in mice lacking astrocytic Bmal1.

Immunofluorescence images of GFAP+ astrocytes in the hippocampus of CTRL-Vehicle, AS-B1KO-Vehicle, and AS-B1KO-SB225002 at 24 h post LPS injection (n = 5 per group). Scale bar, 50 μm.

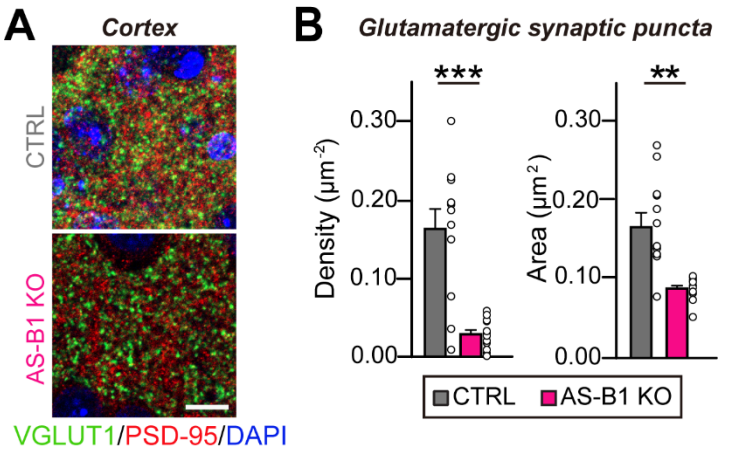

Supplementary Figure S9. Reduced excitatory synaptic puncta in the medial posterior temporal association cortex (MPtA) of LPS-treated astrocytic *Bmal1*-deficient mice

(A) Representative images showing colocalization of VGLUT1 (green) and PSD-95 (red) puncta in the medial posterior temporal association cortex (MPtA) from LPS-treated CTRL and AS-B1 KO mice. Scale bar: 10 µm. (B) Quantification of the density (left) and size (right) of VGLUT1+/PSD-95+ colocalized synaptic puncta in the MPtA. Data are means ±SEMs (**$P < 0.01$, ***$P < 0.001$; Mann-Whitney U test; '*n*' denotes the number of images analyzed; *n* = 10-16 tissues from 4–5 mice per group).

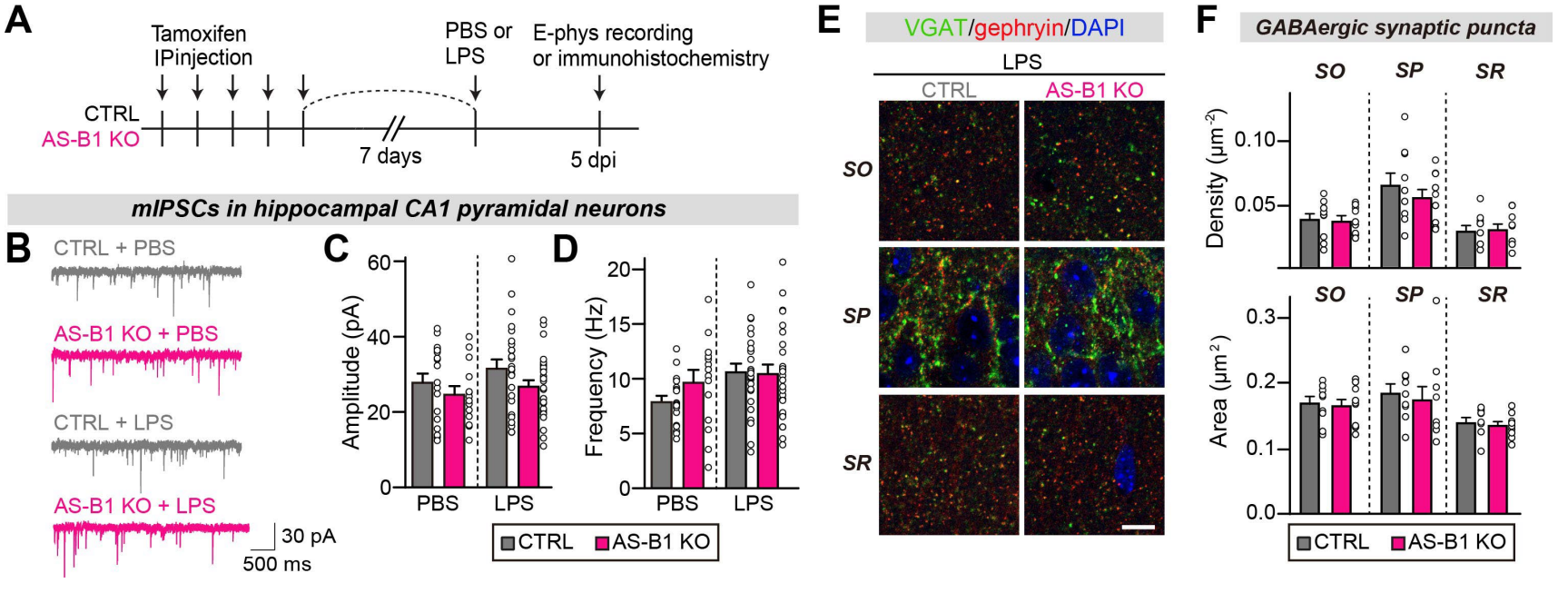

Supplementary Figure S10. Inhibitory synaptic transmission and structure remain unaltered in astrocytic Bmal1-deficient mice

(A) Schematic illustration of the experimental procedure. (B) Representative traces of miniature inhibitory postsynaptic currents (mIPSCs) recorded from CA1 pyramidal neurons in control (CTRL) and astrocytic Bmal1 KO mice (AS-B1 KO) treated with PBS or LPS. (C, D) Summary Graphs showing the amplitude (C) and frequency (D) of mIPSCs. Bar graphs show mean ± SEMs (ANOVA with a non-parametric Kruskal–Wallis test; 'n' denotes the total number of neurons analyzed as follows; CTRL + PBS, n = 19 cells from 3 mice; As-B1 KO + PBS, n = 14 cells from 2 mice; CTRL + LPS, n = 25 cells from 6 mice; As-B1 KO + LPS, n = 27 cells from 6 mice) (E) Representative images showing colocalization of VGAT (green) and gephyrin (red) puncta in the stratum oriens (SO), stratum pyramidale (SP), and stratum radiatum (SR) of the hippocampal CA1 region. Scale bar: 10 µm (F) Quantification of the density (top) and size (bottom) of VGAT+ and gephyrin+ synaptic puncta. Data are means ±SEMs (n = 9 tissues from 3 mice per group; Mann-Whitney U test)

Uncropped gel images

Supplementary Fig S2 G

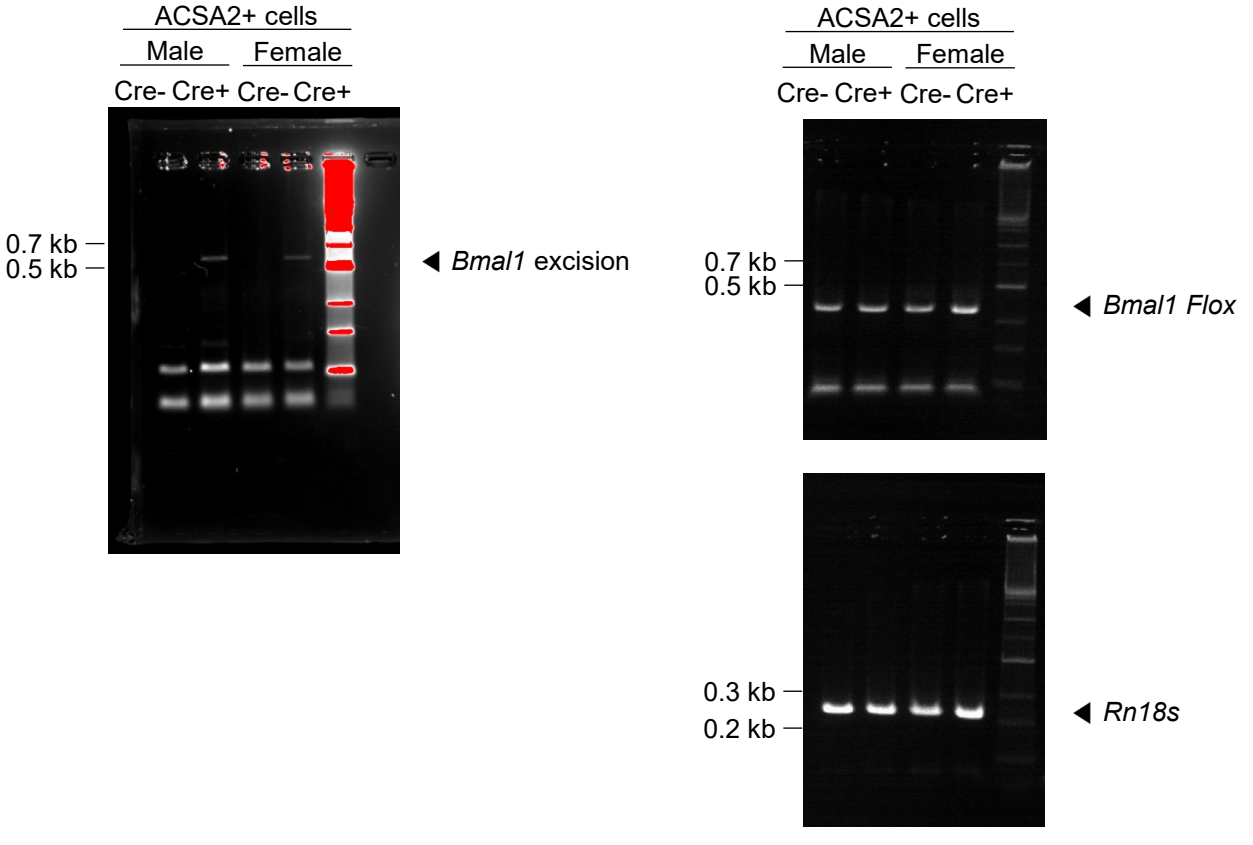

Supplementary Fig S7 C